An Upgraded Measurement of $A^b_{\rm FB}$ from the Charge Asymmetry in Lifetime Tagged Z Decays

Paul Colrain : University of Lancaster, England, UK
Andrew Halley : University of Glasgow, Scotland, UK

July 17, 1996

Abstract

An upgrade of the ALEPH measurement of the $b\bar{b}$ forward-backward asymmetry using lifetime tagging and the hemisphere charge method is presented. All of the LEP-1 data from 1991 to 1995 are analysed as a function of the quark production angle and $b\bar{b}$ purity. Simultaneously fitting the measured forward backward charge asymmetry, mean charge separation together with the total hemisphere and event tagging efficiencies allow precise determinations of the b tag efficiency, charge separation and weak mixing angle, $sin^2\,\theta^{eff}_{\rm w}$. Measuring the b tag efficiency and charge separation in this way leads to increased sensitivity and significant reductions in systematic uncertainties.

1 Motivation

With the completion of LEP-1 data-taking, it is of importance to study how measurements of Z decays can be used to yield maximal sensitivity to electroweak parameters. This contribution presents an improved measurement of the forward-backward asymmetry of b-quarks, $A^b_{\rm FB}$, using the hemisphere charge method in a lifetime tagged sample of hadronic Z decays. The statistical sensitivity of the measurement is increased over that of the previous analysis [1] by fitting both the angular distribution of the quark-antiquark direction relative to the e^+e^- beams and the dependence of the asymmetry on the quark composition as the b-quark purity is increased by a lifetime tag. In addition to this, the measurement benefits from increased statistics by using data from 1991 to 1995 and increasing the angular acceptance[1] from $|\ cos\,\theta\ | \leq 0.8$ to 0.9.

Systematic uncertainties of the previous measurement were dominated by that from the determination of the b-quark hemisphere charge and lifetime tag efficiency. These were determined individually from separate studies. The current analysis simultaneously determines the b hemisphere charge, δ_b and b hemisphere tag efficiency, $\epsilon^{\rm h}_b$. The electroweak sector is fit by a single value; the weak mixing angle, $sin^2\theta^{eff}_{\rm w}$. It is however strongly constrained by two measurable quantities within the analysis, dominated by the asymmetry $A^b_{\rm FB}$ and to a lesser extent by the partial width of Z decays to b quarks, $\mathcal{R}_b$.

2 Data Sample and Selection Criteria

Data from the LEP-1 period, where silicon vertex detector (VDET) tracking was available, are used from 1991 to 1995. After hadronic event selection based on charged tracks, the thrust axis is computed using the ENFLW algorithm which combines charged and neutral information from the ALEPH tracking detectors and calorimeters. Further event selection demands that the thrust axis determination is successful and that there is at least one charged track per hemisphere. Subsequent to this the lifetime tagging algorithm, QIPBTAG, is applied to select events with

[1] This is defined in terms of the polar angle of the thrust axis, θ, relative to the incoming beams in the detector.

at least two jets having greater than 10 GeV momentum and inside the polar acceptance of VDET. This leaves 4.025 million events out of a total of 4.104 million which pass the hadronic event selection. The statistics of the event selection are detailed in Table 1. The measurement

Selection Criteria	*Year 1991*	*1992*	*1993*	*1994*	*1995*	*Total*
Hadronic Selection	0.249	0.681	0.678	1.749	0.749	4.104
High Voltage Checks	0.243	0.671	0.672	1.724	0.736	4.047
Thrust Calculation	0.243	0.671	0.672	1.724	0.736	4.046
Track in Each Hemisphere	0.242	0.670	0.670	1.720	0.734	4.036
Lifetime Tag Selection	0.241	0.668	0.668	1.716	0.732	4.025

Table 1: *Summary of selected events ($\times 10^6$) after each stage of the event selection for the various years considered.*

acceptance is defined by selecting events with polar angle of the thrust axis, $\mid cos\,\theta \mid$ less than 0.9 which is then divided into independent bins of $cos\,\theta$ with width 0.1. The lifetime tag is applied to both hemispheres of the event and accepted if either tags lie within the hemisphere tag probabilty windows given in Table 2. All subsequent measurements are performed using this

Window Number	*Probability Window Range*	*Bin Centre (-log$_{10}$)*	*b Purity (in %)*	*c Purity (in %)*	*Fraction of Events*
1	1.0 $\rightarrow$ 0.1	0.26	6.7%	14.8%	61.1%
2	0.1 $\rightarrow$ 0.032	1.18	19.6%	24.6%	13.4%
3	0.032 $\rightarrow$ 0.005	1.73	37.8%	28.8%	9.8%
4	0.005 $\rightarrow$ 0.001	2.52	60.9%	24.6%	4.4%
5	0.001 $\rightarrow$ 0.0001	3.26	79.0%	15.4%	3.8%
6	0.0001 $\rightarrow$ 0.000001	5.26	92.6%	5.7%	4.3%
7	0.000001 $\rightarrow$ 0.0	5.30	99.0%	0.7%	3.2%

Table 2: *Summary of bin ranges, purities and fraction of the events selected based on expectation from Monte Carlo simulation.*

matrix of independent bins of $cos\,\theta$ and lifetime tag probability.

3 Principles of the Method

The principles of the hemisphere charge method and lifetime tagging procedure are described in detail in [1, 2] and only modifications and extensions of the method are described here. The hemisphere charges are measured using a longitudinal momentum weighting scheme with κ parameters 0.3, 0.5, 1.0, 2.0 and ∞ in each of the forward ($+z$) and backward hemispheres of the ALEPH detector. For each bin in $cos\,\theta$ and lifetime tag probability the following measurements are performed using the hemisphere charge quantities :

1. The mean charge asymmetry :

$$< Q_{\rm FB} > = \frac{\sum_{f=u,d..}^{b} \mathcal{R}_f\, \epsilon_f^{\rm e}\, \delta_f\, A_{\rm FB}^f}{\sum_{f=u,d..}^{b} \mathcal{R}_f\, \epsilon_f^{\rm e}} \qquad (1)$$

2. The mean charge separation :

$$\bar{\delta}^2 \;=\; -4\cdot < Q_{\rm F}Q_{\rm B} > = \frac{\sum_{f=u,d..}^{b} \mathcal{R}_f\, \epsilon_f^{\rm e}\, \bar{\delta}_f^2}{\sum_{f=u,d..}^{b} \mathcal{R}_f\, \epsilon_f^{\rm e}} \tag{2}$$

3. The total hemisphere tagging efficiency :

$$\epsilon^{\rm h} \;=\; \sum_{f=u,d..}^{b} \mathcal{R}_f\, \epsilon_f^{\rm h} \tag{3}$$

4. The total event tagging efficiency :

$$\epsilon^{\rm e} \;=\; \sum_{f=u,d..}^{b} \mathcal{R}_f\, \epsilon_f^{\rm e} \tag{4}$$

where the following definitions have been used for the relationship between the mean charge separation for a given flavour f, δ_f and $\bar{\delta_f}$:

$$\begin{aligned} \bar{\delta}_{\rm f}^2 \;&=\; -4\langle {\rm Q_F Q_B}\rangle_{\rm f} \;\; - \langle {\rm Q_{FB}}\rangle_{\rm f}^2 \;+\; \langle {\rm Q}\rangle_{\rm f}^2 \\ &=\; \delta_{\rm f}^2 \;-\; 4\langle \mathcal{R}_{\rm f}\mathcal{R}_{\bar{\rm f}}\rangle \;\; - \langle {\rm Q_{FB}}\rangle_{\rm f}^2 \\ &=\; \left[\delta_{\rm f}\,(1+k_{\rm f})\right]^2 . \end{aligned} \tag{5}$$

and the hemisphere and event tagging efficiencies :

$$\epsilon_f^{\rm e} \;=\; 2\epsilon_f^{\rm h}\left(1 \;-\; \rho_f\,\epsilon_f^{\rm h}\right) \;+\; \rho_f\,\left(\epsilon_f^{\rm h}\right)^2 \tag{6}$$

where $\epsilon_f^{\rm e}$ is the efficiency to tag at least one of the two event hemispheres. The tag correlation, ρ_f, represents that between the two hemisphere tags of an $f\bar{f}$ event, whereas k_f is the correlation between the hemisphere charge measurements.

In order to calculate the theoretical expectations for each of the measured quantities, it is necessary to have estimates of the hemisphere tagging efficiencies for charm and light-quark flavours, $\epsilon_f^{\rm c}$ and $\epsilon_f^{\rm uds}$. Similarly, correlations between the hemisphere tag probabilities in b events, ρ_f, for b quarks[2] and that between hemisphere charges, k_f, are also inputs to the method. These correlations are calculated using Monte Carlo simulation.

Initially, the simulation provides an over-optimistic estimate of track impact-parameter distributions and so $cos\,\theta$ and momentum dependent smearing is applied in a generalisation of the method used in [2]. Decay modes of charm mesons are also reweighted in the Monte Carlo to bring them in line with recent measurements. These corrections induce a substantial improvement in the overall agreement between data and simulation and are applied separately for each year of data taking using the appropriate Monte Carlo production when available. Hemisphere tagging efficiencies for simulated events are given in Table 3 together with the event tagging efficiencies for b events.

Hemisphere charge correlations and their systematic uncertainties are taken from [3] and are given in Table 4. Charge separations for charm and light-quark flavours are needed, although their contributions are reduced significantly by the lifetime tag. Fitted values are available from [3] and are summarised in Table 5 as a function of κ together with their systematic uncertainties constrained by jet charge measurements in data.

Physical quantities which depend on the electroweak sector such as the partial widths of the Z, $\mathcal{R}_f$, and the asymmetries, $A_{\rm FB}^f$, are calculated within the context of the Standard Model using ZFITTER calculations [4]. Radiative QCD corrections are deactivated in ZFITTER as they are taken into consideration in the determination of the the charge separations as described in [5].

[2] Where this is may be written as $\rho_f \;=\; \lambda_f\left(1/\epsilon_f^{\rm h} - 1\right) + 1$ and λ_f is the "classical" correlation between hemisphere tags in the same event[2].

Window Number	*uds Hem. Tag Efficiency*	*c Hem. Tag Efficiency*	*b Hem. Tag Efficiency*	*b Event. Tag Efficiency*
1	1.000	1.000	1.000	1.000
2	0.074	0.142	0.217	0.381
3	0.030	0.099	0.203	0.353
4	0.006	0.034	0.112	0.207
5	0.002	0.019	0.106	0.197
6	0.001	0.008	0.110	0.203
7	0.000	0.001	0.071	0.135

Table 3: *Input values from the simulation of single hemisphere and event tagging efficiencies and their correlations in the lifetime tag selection windows.*

κ	u	d	s	c	b
0.3	15.3 ± 2.5	30.8 ± 4.4	26.6 ± 3.5	15.4 ± 2.7	36.4 ± 3.6
0.5	8.6 ± 1.1	14.8 ± 3.3	11.6 ± 2.3	8.5 ± 2.5	18.4 ± 2.3
1.0	5.5 ± 1.2	4.7 ± 1.9	5.4 ± 1.1	2.2 ± 1.1	8.9 ± 1.1
2.0	5.3 ± 1.0	3.7 ± 1.8	4.9 ± 1.2	1.2 ± 3.6	8.1 ± 1.8
∞	5.8 ± 1.3	4.7 ± 3.8	5.1 ± 1.8	0.0 ± 8.8	6.5 ± 3.6

Table 4: *The corrections k_f in percent for u, d, s, c and b quarks for various κ values. The combined statistical and systematic error is given.*

4 Fit Procedure

The four measured quantites ($Q_{\rm FB}$, $\bar{\delta}$, $\epsilon^{\rm h}$, $\epsilon^{\rm e}$) are fitted simultaneously in each bin of $cos\,\theta$ and hemisphere tag window[3] as a function of three independent variables; (a) δ_b, (b) $\epsilon_b^{\rm h}$ and (c) the weak mixing angle, $sin^2\,\theta_{\rm w}^{eff}$. The latter is varied in the fit by altering the mass of the top quark, $m_{\rm t}$, which is used to perform the calculations of electroweak radiative corrections. In effect, this leaves one degree of freedom per bin with which to test the hypothesis that the data are consistent with the Standard Model.

One of the significant improvements of the current analysis over that used previously is that it allows the fit to be extended into regions of detector acceptance where both the hemisphere tagging efficiencies and charge calculations are known to be degraded. As the mean charge separation is now fitted fitted to data, the precise degree of degradation is observed and used to fit the high $cos\,\theta$ region with little increase in systematic uncertainties.

Experimental results for the four measured quantities in 1991 $\rightarrow$ 1995 data are shown in Figure 1 as a function of $cos\,\theta$ and two different hemisphere tag windows for comparison. The four measured quantities are fitted simultaneously in each angular and lifetime tag window. Each quantity generally constrains a different quantity. ie. Figure 1(a) and (b) tightly constrain the event purities and the angular acceptance. It is clear that expectations of the smeared Monte Carlo simulation for event and hemisphere tagging efficiencies accurately fit the data, including the low angle region. Figure 1(c) is used to constrain the charge separations. At low purities this contains a mixture of light and heavy quarks, whereas at high purities it is dominated by δ_b. As a consequence the dominant free parameter fitted by the distributions shown in Figure 1(d) is the underlying asymmetry itself. The fitted curves represent a parameterisation of the bin-by-bin fits to the asymmetry in data. In all cases, theoretical expectations for all measured quantites

[3] Using the method of Lagrange Multipliers.

κ	δ_u		δ_d		δ_s		δ_c	
0.3	$+0.238$	± 0.006	-0.143	± 0.006	-0.171	± 0.002	$+0.192$	± 0.009
0.5	$+0.291$	± 0.007	-0.171	± 0.007	-0.218	± 0.003	$+0.200$	± 0.010
1.0	$+0.406$	± 0.009	-0.229	± 0.011	-0.329	± 0.005	$+0.211$	± 0.016
2.0	$+0.528$	± 0.011	-0.289	± 0.015	-0.455	± 0.009	$+0.208$	± 0.026
∞	$+0.621$	± 0.013	-0.339	± 0.018	-0.557	± 0.011	$+0.194$	± 0.035

Table 5: *Charm and light-quark charge separations as a function of the longitudinal momentum weighting parameter, κ.*

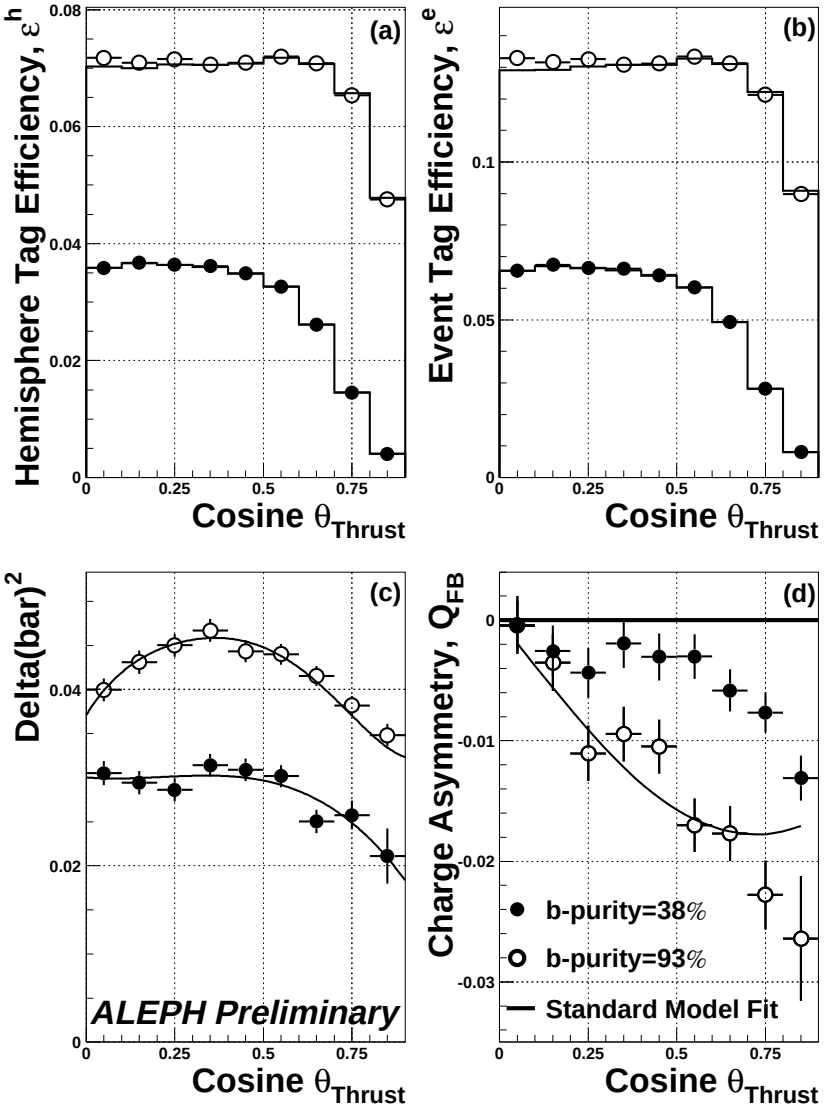

Figure 1: *Measured quantities used in the fit (a) Single hemisphere tagging efficiency, (b) event tagging efficiency, (c) $\bar{\delta}^2$ and (d) the charge asymmetry, $< Q_{\rm FB} >$ as a function of polar angle for examples of two lifetime tag b purities. The data are indicated as points with the Standard Model fit results indicated by solid lines.*

are in good agreement with data.

The distributions of tagging efficiency and charge separation with angle vary strongly at low angles, close to the beam. This confirms the necessity of fitting to the mean charge seperation as a function of angle to remove any bias this might cause. Monte Carlo studies indicate that it is primarily the wider b jets which are degraded at low angles, whereas light-quark and charm events suffer little observable effects.

5 Experimental Results

It is clear from Figure 1 that the increase in acceptance from 0.8 to 0.9 is responsible for a significant improvement in measurement sensitivity. The low tagging efficiency in this region being compensated for by the large asymmetries at large $cos\,\theta$.

An apparent discrepancy in the single hemisphere and event tagging efficiencies is observed for all tag windows with low b-purities. This is thought most likely to be due to an incorrect expectation for the charm hemisphere tagging efficiency, $\epsilon_c^{\rm h}$ as it appears most strongly in the tag windows which are neither dominated by light-quarks or at high b-purities. This is detected in the fit procedure by noting that the inclusion of distributions from the low b-purity tag windows leads to an increase in the χ^2 beyond the limit expected a the level of 95% confidence. For this reason, only tag windows 5, 6 and 7 are currently used for the following results.

The fits to electroweak parameters are given in Table 6 for the years 1991 to 1995 individually, which are then combined. The final χ^2 distribution for all 1991 $\rightarrow$ 1995 data is shown in Figure 2

Year	$A_{\rm FB}^b$		m_t	$sin^2\,\theta_{\rm w}^{eff}$	
1991	0.0857	$\pm$0.0152	$99^{+95}_{-99}\ GeV/c^2$	0.2343	$\pm$0.0027
1992	0.0999	$\pm$0.0102	$189^{+45}_{-60}\ GeV/c^2$	0.2317	$\pm$0.0018
1993	0.0859	$\pm$0.0081	$101^{+55}_{-55}\ GeV/c^2$	0.2342	$\pm$0.0014
1994	0.0947	$\pm$0.0056	$161^{+28}_{-36}\ GeV/c^2$	0.2326	$\pm$0.0010
1995	0.0887	$\pm$0.0087	$122^{+54}_{-74}\ GeV/c^2$	0.2337	$\pm$0.0016
Total	0.0927	$\pm$0.0039	$149^{+22}_{-25}\ GeV/c^2$	0.2330	$\pm$0.0007

Table 6: *Summary of fitted electroweak parameters for years 1991 to 1995 and the combined fitted value of* $sin^2\,\theta_{\rm w}^{eff}$.

which yields the value :

$$sin^2\,\theta_{\rm w}^{eff} \;=\; 0.2330 \;\pm\; 0.0007$$

where the error contains contributions from the statistical and systematic uncertainties in the input distributions of tagging efficiencies and dependence on polar angle. The total χ^2 is 158 for 135 degrees of freedom. The stability of the results as a function of κ is shown in Figure 3 indicating the stability of the measurement over a wide range of momentum scales.

6 Systematic Uncertainties

Many of the systematic uncertainties listed separately in the previous analysis have been incorporated directly into the one presented here. By simultaneously fitting to the single and total event tagging efficiencies, the statistical and systematic errors on the acceptance are already incorporated. The remaining systematic error contributions are listed in Table 7. Several of these remain to be re-evaluated in the context of the current analysis. Consequently they represent a strongly conservative overestimate of the systematic uncertaintiesand the reported result should

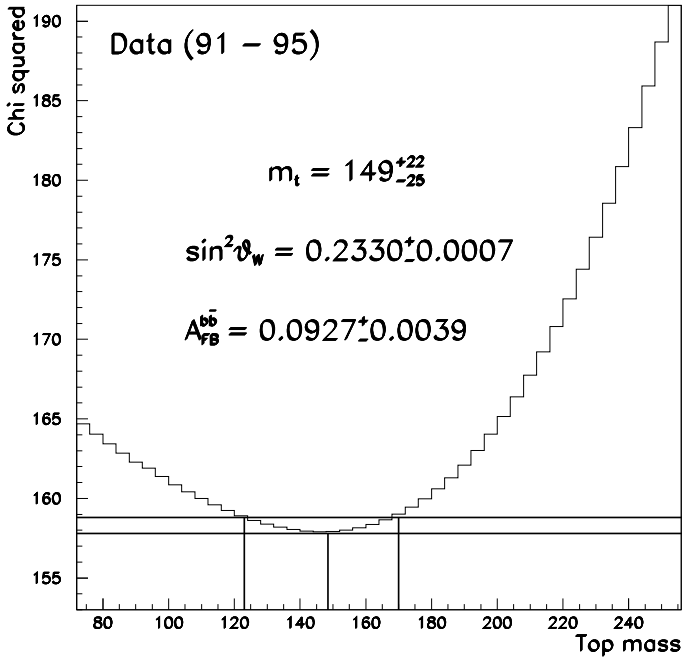

Figure 2: *Combined χ^2 distribution for the* 1991 $\rightarrow$ 1995 *data as a function of the electroweak parameter, m_t, used in the fit to the data.*

be viewed as preliminary. This is most striking in the example of the systematic error due to the tag purity. The quoted value is based upon selecting events with hemisphere probabilities less than 0.005 whereas the current method analyses events within a sequence of continuous ranges of probability. The remaining errors arise from the incomplete knowledge of the light-quark separations and hemisphere charge correlations which however remain small.

7 Conclusion

The forward-backward asymmetry for b quarks at the Z peak is measured using an upgraded version of the lifetime tag and hemisphere charge method. The combined result for the 1991 to 1995 data is :

$$sin^2\,\theta_{\rm w}^{eff} \;=\; 0.2330 \;\pm\; 0.0009$$

which corresponds to a b forward-backward asymmetry of :

$$A_{\rm FB}^{b} \;=\; 0.0927 \;\pm\; 0.0039\,(stat.) \;\pm\; 0.0034\,(syst.)$$

The fitting procedure currently does not make full use of the statistical senstivity available as it does not make use of the semi-independent κ values and/or include a simultaneous fit of the tag regions towards lower b-purities. Both additions are likely to improve the final error estimate as will a thorough re-evaluation of the systematic errors due to uncertainties on the lifetime tag purities.

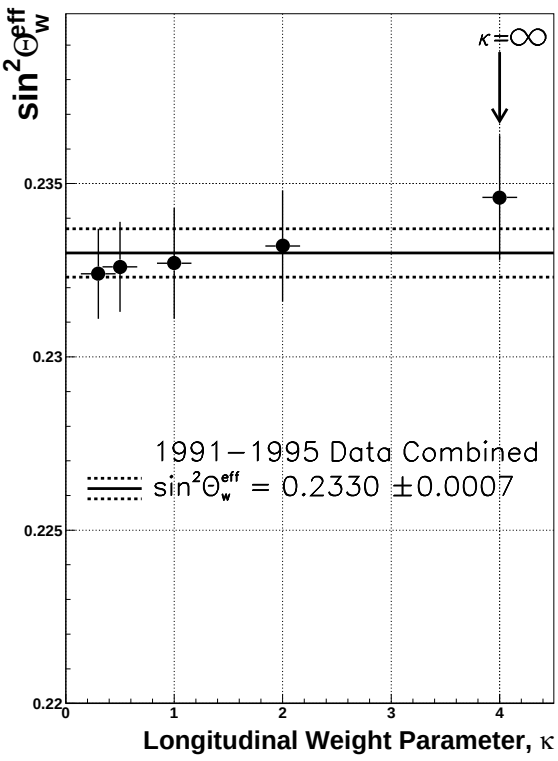

Figure 3: *Variation of extracted weak mixing angle as a function of* κ. *Note that errors on each measured point are correlated with others.*

References

[1] ALEPH Collaboration, D. Buskulic et al, Physics Letters B335(1994) 99.

[2] ALEPH Collaboration, D. Buskulic et al, Physics Letters B313(1993) 535.

[3] ALEPH Collaboration, D. Buskulic et al, CERN PPE 96-017, (1996).
(Submitted to Zeitschrift fuer Physik C)

[4] D. Bardin et al, CERN TH 6443-92, (1992).

[5] The LEP Collaborations, CERN PPE 96-017, (1996).

Source of Systematic Error	$\Delta sin^2\,\theta_{\rm w}^{eff}$
Systematic Error from knowledge of δ_u	0.0001
Systematic Error from knowledge of δ_d	0.0001
Systematic Error from knowledge of δ_s	0.0001
Systematic Error from knowledge of δ_c	0.0002
Systematic from hemisphere charge correlations	0.0003
Stat. and Syst. Error on Tag Purity	0.0004
Experimental Systematics	0.0003
Systematic from Thrust Axis Resolution	0.0001
Total Systematic Error	0.0006

Table 7: *Summary of systematic uncertainties on* $sin^2\,\theta_{\rm w}^{eff}$ *from the fit. The second category of errors remain to be recalculated for the purposes of the current analysis.*